

**Journal:** Hydrology and Earth System Sciences

**Title:** Assimilating Shallow Soil Moisture Observations into Land Models with a Water Budget Constraint

**Authors:** Bo Dan, Xiaogu Zheng, Guocan Wu, and Tao Li

**MS NO.:** hess-2019-696

**MS Type:** Research Article

The authors highly appreciate the anonymous reviewer for his/her very helpful and insightful comments that lead to the considerable improvement of the quality of this manuscript. We have checked our work carefully according to these comments and made the requested changes. The main improvement is the discussions on updating the canopy water content and WCEnKF in reducing water budget residual. The Abstract and Conclusions sections are also revised with adding necessary quantitative measures.

Below we indicate the comments and use blue font for our responses. The corresponding revised texts are also used blue font in the revised version of our manuscript.

The study is suitable for publication after following minor changes.

(1) Both reviewers the prior version of the manuscript asked about the direct update of canopy water content. I understand that the authors are following the approach of Yilmaz et al. (2011; 2012) but this choice of updating canopy water content needs to be discussed further in the manuscript. It could be done in the discussion section or in the methods section.

**Response:** Thanks for your comment. The canopy's water content (CWC) and snow water equivalent (SWE) are related to the water budget. If the water budget constraint is absent, they are normally not updated and the vegetation module transports the water into the vegetation layer. However, the present study focused on the assimilation with the water budget constraint, then updating CWC and SWE would help to reduce the water budget residuals.

For the assimilation with the water budget constraint but without update of CWC and SWE, the state variables related to the water budget are decomposed as  $\mathbf{x} = (\mathbf{x}_1, \mathbf{x}_2)$  where  $\mathbf{x}_1$  comprises of SM and SIC (the soil moisture content and the soil ice content at the 10 vertical levels listed in Table 1),  $\mathbf{x}_2$  comprises of CWC and SWE (the canopy's water content and the snow water equivalent).  $\mathbf{c} = (\mathbf{c}_1, \mathbf{c}_2)$  is a 22-dimensional vector that converts the units of  $\mathbf{x} = (\mathbf{x}_1, \mathbf{x}_2)$  to millimeters (mm). The assimilation for not update of  $\mathbf{x}_2$  can be achieved by substituting  $\mathbf{x}$  and  $\beta_{n,t}$  in section 3.2 by  $\mathbf{x}_1$  and  $\beta_{n,t}$  respectively, that is

$${}_1\beta_{n,t} = {}_1\mathbf{c}^T {}_1\mathbf{x}_{n,t-1}^a + {}_2\mathbf{c}^T {}_2\mathbf{x}_{n,t-1}^f + Pr_t - Ev_{n,t}^f - Rn_{n,t}^f, \quad (22)$$

where  $Pr_t$ ,  $Ev_{n,t}^f$  and  $Rn_{n,t}^f$  are diagnostic variables specifying the states of the precipitation, evapotranspiration and runoff, respectively. By this way, the canopy's water content are not updated and the vegetation module transports the water into the vegetation layer. In this study, the range of the estimated CWCs for all assimilations with or without update of  $\mathbf{x}_2$  is only about 0.005 mm. Considering the estimated water budget residuals are between 0.05 mm and 0.14 mm and there is no SWE in the summer period, we conclude that update of CWC has a little impact on water balance in this study.

This discussion was added in section 6.3 of the revised version. (Lines 539-561)

(2) The results in Fig. 6 indicate that WcEnKF results in the smallest water balance residual relative to various WcEnKF-Inf and WcEnKF-Inf-Loc. I realize that WcEnKF-Inf and WcEnKF-Inf-Loc leads to smaller bias in soil moisture but if the focus of a study or experiment is reducing water balance, does this result indicate that WcEnKF is a better choice? I assume it is computationally faster to implement WcEnKF too. Please discuss this point.

**Response:** Thanks for your comment. We agree that if the focus of a study or experiment is reducing water balance, WcEnKF could be a better choice and computationally faster than WcEnKF-Inf and WcEnKF-Inf-Loc schemes. Accordingly, it is plainly obvious that the water balance residual of the scheme WcEnKF-Inf is larger than that of the scheme WcEnKF. However, the objective in this study is to reduce water balance without significantly increasing the analysis error. Since the analysis errors for WcEnKF in the layers shallower than 36.6 cm are significantly larger than those for the schemes with inflation, WcEnKF is not preferred.

These texts have been added to the revised version. (Lines 468-476)

(3) Both Abstract and Conclusions section do not mention any quantitative measures (e.g. % improvement in bias) of improvement in model performance after data assimilation.

**Response:** Thanks for your comment. The main quantitative measures of the analysis errors and water budget residuals are included in the abstract and conclusions.

For the more details, in abstract we added (Lines 27-35):

“The results of the assimilation process suggest that the inflation approach effectively reduces the analysis error from 6.70% to 2.00% in shallow layers, but increases from 6.38% to 12.49% in deep layers. The vertical localization approach leads to 6.59% of the analysis error in deep layers, and the bias-aware assimilation scheme further reduces to 6.05% . The spatial average of the water balance residual is 0.0487 mm of weakly constrained EnKF scheme, and 0.0737 mm of weakly constrained EnKF with inflation and localization scheme, which are much smaller than 0.1389 mm of the EnKF scheme.”

In the conclusion we added (Lines 589-593):

“The experiment results of synthetic study show that the WcEnKF-Inf-Loc assimilation scheme can reduce the analysis error from 6.70% to 2.00% in the shallow

layers, with both the short-lived analysis error and the analysis bias reduced. It also leads to a rational water budget residual with spatial average 0.0737 mm, which is much smaller than 0.1389 mm of the EnKF scheme.”

(4) Line 29: "Finnaly" should be "Finally".

**Response:** Revised.

(5) Line 78: "it suggests" should be "it is suggested".

**Response:** Revised.

(6) 4.2.3, please define the variables in the equation to calculate water balance residuals.

**Response:** The variables are defined as follows: “ $N$  is the ensemble size,  $a_{ts}$  is the number of assimilation time steps, and  $r_{n,t}$  is the ensemble water budget residual at time step  $t$  as defined in Eq. (6).”

This was added in section 4.2.3. (Lines 361-362)

(7): 6.3 "Notes" is a pretty vague heading for this section, perhaps "Broader implications" or "Global implementation" would be better.

**Response:** The heading has been changed to “Broader implications”.

Again, thanks for your valuable comments and recommendation.

The main changes are listed as follows.

(1) Lines 27-35: Added the main quantitative measures of the analysis errors and water budget residuals in the abstract.

(2) Lines 361-362: Added the variables in the equation to calculate water balance residuals (Eq. (21)).

(3) Lines 468-476: Added the discussion on WCEnKF scheme.

(4) Lines 539-561: Added the discussion on updating of canopy water content.

(5) Lines 589-593: Added the main quantitative measures of the analysis errors and water budget residuals in the conclusions.

1     **Assimilating Shallow Soil Moisture Observations into Land Models**  
2                     **with a Water Budget Constraint**

3

4                     Bo Dan<sup>1</sup>, Xiaogu Zheng<sup>2</sup>, Guocan Wu<sup>3\*</sup>, and Tao Li<sup>4</sup>

5

6     <sup>1</sup> National Marine Data and Information Service, Tianjin, China

7     <sup>2</sup>Key Laboratory of Regional Climate-Environment Research for East Asia, Institute  
8     of Atmospheric Physics, Chinese Academy of Sciences, Beijing, China

9     <sup>3</sup>College of Global Change and Earth System Science, Beijing Normal University,  
10    Beijing, China

11    <sup>4</sup>Institute of Statistics, Xi'an University of Finance and Economics, Xi'an, China

12

---

\*Corresponding author: Guocan Wu  
E-mail: gcwu@bnu.edu.cn

13 **Abstract**

14 Assimilating observations of shallow soil moisture content into land models is an  
15 important step in estimating soil moisture content. In this study, several modifications  
16 of an ensemble Kalman filter (EnKF) are proposed for improving this assimilation. It  
17 was found that a forecast error inflation-based approach improves the soil moisture  
18 content in shallow layers, but it can increase the analysis error in deep layers. To  
19 mitigate the problem in deep layers while maintaining the improvement in shallow  
20 layers, a vertical localization-based approach was introduced in this study. During the  
21 data assimilation process, although updating the forecast state using observations can  
22 reduce the analysis error, the water balance based on the physics in the model could  
23 be destroyed. To alleviate the imbalance in the water budget, a weak water balance  
24 constrain filter is adopted.

25 The proposed weakly constrained EnKF that includes forecast error inflation and  
26 vertical localization was applied to a synthetic experiment. An additional bias-aware  
27 assimilation for [reducing](#) the analysis bias is [also](#) investigated. [The results of the](#)  
28 [assimilation process suggest that the inflation approach effectively reduces the](#)  
29 [analysis error from 6.70% to 2.00% in shallow layers, but increases from 6.38% to](#)  
30 [12.49% in deep layers. The vertical localization approach leads to 6.59% of the](#)  
31 [analysis error in deep layers, and the bias-aware assimilation scheme further reduces](#)  
32 [to 6.05% . The spatial average of the water balance residual is 0.0487 mm of weakly](#)  
33 [constrained EnKF scheme, and 0.0737 mm of weakly constrained EnKF with inflation](#)  
34 [and localization scheme, which are much smaller than 0.1389 mm of the EnKF](#)  
35 [scheme.](#)

36  
37 **Keywords** soil moisture, water balance, data assimilation, forecast error inflation,

38 vertical localization

39



## 40 **1. Introduction**

41 Soil moisture content is one of the most important variables that affect the water  
42 cycle and energy balance through land-atmosphere interactions, especially  
43 evaporation and precipitation (Han *et al.* 2014; Kumar *et al.* 2014; McColl *et al.* 2019;  
44 Pinnington *et al.* 2018). Adequate knowledge of the horizontal and vertical  
45 distributions of soil moisture at sub-seasonal to seasonal time scale could improve  
46 weather and climate predictions (Delworth and Manabe 1988; Pielke 2001).  
47 Alongside snow cover, soil moisture content is an important component of the  
48 meteorological memory of the climate system over land (McColl *et al.* 2019; Robock  
49 *et al.* 2000; Zhao and Yang 2018). It is also a primary water resource for the terrestrial  
50 ecosystem and affects runoff (GUSEV and Novak 2007).

51 There are several ways to estimate the soil moisture content. Land surface  
52 models can provide temporally and spatially continuous estimates of the soil moisture  
53 content, but limited by the uncertainty in the models' parameters, errors in the forcing  
54 data and imperfect physical parameterizations (Bonan 1996; Dai *et al.* 2003;  
55 Dickinson *et al.* 1993; Oleson *et al.* 2010; Yang *et al.* 2009). Compared with the  
56 results of models, in-situ observations of the soil moisture content provide more  
57 accurate profiles (Bosilovich and Lawford 2002; Dorigo *et al.* 2011; Robock *et al.*  
58 2000); however, networks of in-situ observations are usually too sparse to estimate the  
59 soil moisture content on a regional scale (Gruber *et al.* 2018; Loizu *et al.* 2018).  
60 Satellite remote sensing retrievals could provide soil moisture content data on regional  
61 scales (Bartalis *et al.* 2007; Crow *et al.* 2017; Entekhabi *et al.* 2010; Kerr *et al.* 2010;  
62 Lu *et al.* 2015; Njoku *et al.* 2003), but they are only available for the shallow layer of  
63 the soil and the quality is poor in vegetated area (Pinnington *et al.* 2018; Yang *et al.*  
64 2009).

65 Many studies indicated that a better approach to improving the estimates of soil  
66 moisture contents on regional scales is to constrain land model predictions by  
67 assimilating surface soil moisture data (Crow and Loon 2006; Crow and Wood 2003;  
68 Reichle and Koster 2005). It can provide better estimates of the true soil moisture  
69 content column states than the model forecasts (Crow *et al.* 2017; Lu *et al.* 2012; Lu  
70 *et al.* 2015), and can further improve land surface model initial conditions for coupled  
71 short-term weather prediction (Chen *et al.* 2014; Santanello *et al.* 2016; Yang *et al.*  
72 2016). Especially, surface soil moisture data can be provided by in-situ observations  
73 and passive microwave measurements (brightness temperatures) observed by remote  
74 sensing.

75 A good estimate of the forecast error covariance matrix is crucial for the  
76 compromise between uncertain observations and imperfect model predictions in data  
77 assimilation (Anderson and Anderson 1999; Miyoshi 2011; Miyoshi *et al.* 2012; Wang  
78 and Bishop 2003). For the Ensemble Kalman Filter (EnKF) assimilation method, the  
79 forecast error covariance matrix is estimated using the sample covariance matrix of  
80 the ensemble forecasts (Dumedah and Walker 2014; Evensen 1994; Han *et al.* 2014).  
81 However, it is usually underestimated due to sampling and model errors, which can  
82 eventually results in filter divergence (Anderson and Anderson 1999; Constantinescu  
83 *et al.* 2007; Yang *et al.* 2015). To address this problem, it is suggested that the forecast  
84 covariance matrix be multiplied by a factor (Dee and Da Silva 1999; Dee *et al.* 1999;  
85 Li *et al.* 2012; Zheng 2009). This approach is referred to as inflation, and it becomes  
86 particularly important when the error in the model is large (Bauser *et al.* 2018; El  
87 Gharamti *et al.* 2019; Liang *et al.* 2012; Raanes *et al.* 2019; Wu *et al.* 2013).  
88 Therefore, it could work well in this situation because of the enormous errors in the  
89 land model.

90 In this study, a scheme for assimilating synthetic observations of the soil  
91 moisture content into land models was developed based on EnKF method, which can  
92 provide a foundation for further satellite data assimilation. For the synthetic  
93 experiment, the Version 4.0 of the Community Land Model (CLM 4.0, (Lawrence *et*  
94 *al.* 2011; Oleson *et al.* 2010)) was used to generate the “true values” and the Common  
95 Land Model (CoLM, (Dai *et al.* 2003)) was selected as the forecast operator. The  
96 differences in these two models are referred to the model error in an imperfect land  
97 surface model. The inflation factors are estimated at every observation time step  
98 during the assimilation process by minimizing the -2log-likelihood of the difference  
99 between the forecast and the observation (Liang *et al.* 2012; Zheng 2009). For  
100 assimilating observations near the surface only, such inflation approach can improve  
101 the estimates of the forecast error statistics in shallow soil layers but may artificially  
102 enlarge the forecast error statistics in deep soil layers. To avoid the possibility of  
103 decreasing the quality of the estimates in deep soil layers, a vertical localization with  
104 weighting of observations is adopted (Janjić *et al.* 2011). In this approach, a  
105 localization function multiplies the weights on the components of the state vector  
106 according to the distance from state layer to the observation. Moreover, the method  
107 based on the maximum likelihood estimation was proposed to estimate the optimal  
108 localization scale factor.

109 A major objective of soil moisture data assimilation is to address biases in  
110 models and observations (Koster *et al.* 2009; Reichle and Koster 2004). In this study,  
111 we only assume that models could be biased, while the soil moisture observations are  
112 assumed to be unbiased. Moreover, the soil moisture observations are restricted in  
113 shallow layer, so there is no observation available to directly correct the modeled soil  
114 moisture biases in deep layers. However, bias can be detected by monitoring

115 observation-minus-forecast statistics in the assimilation system (Dee and Todling  
116 2000). Then a bias-aware assimilation method can be designed to estimate and correct  
117 the systematic errors sequentially with the model state variables (Dee 2005). Such  
118 bias correction method is adopted in this study to detect the performance among  
119 different assimilation schemes. Furthermore, the analysis error is decomposed to a  
120 short-lived error (random error) and a bias (system error). It demonstrates that the  
121 proposed scheme can reduce the both for soil moisture in shallow layers. These  
122 improvements steps can also result in a reasonable estimates of the soil moisture  
123 content in the deep layers.

124 In addition to improve assimilation accuracy, this study also focuses on the  
125 imbalance in the water budget that occurs during the process of assimilating the soil  
126 moisture data. The terrestrial water budget is a key part of the global hydrologic cycle.  
127 A better understanding of the budget can help us to improve our knowledge of  
128 land-atmosphere water exchange and related physical mechanisms and therefore, can  
129 improve our ability to develop models (Pan and Wood 2006). Generally speaking,  
130 analyses do not conserve the water budget due to inconsistencies between predictions  
131 made by models and observations (Li *et al.* 2012; Pan and Wood 2006; Wei *et al.*  
132 2010; Yilmaz *et al.* 2011; Yilmaz *et al.* 2012). It is really a problem if the water  
133 balance is violated in a systematic manner (for example, model is biased), which  
134 suggests a trouble in data assimilation. Pan and Wood (2006) proposed a method  
135 based on a strong constraint to reincorporate the water balance. However, this method  
136 redistributes the error among the different terms in the water budget, which could  
137 result in unrealistic estimates (Pan and Wood 2006; Yilmaz *et al.* 2011).

138 To overcome this shortcoming, Yilmaz *et al.* (2011) proposed using a weakly  
139 constrained ensemble Kalman filter (WCEnKF) to reduce the imbalance in the water

140 budget. In a synthetic study, they concluded that the accuracy of a WCEnKF-based  
141 analysis is close to that of an EnKF-based analysis but the water budget balance  
142 residuals are much smaller than that of an unconstrained filter. Nevertheless, the  
143 observations of the soil moisture content cover the entire column, and a perfect model  
144 was used in their studies. This is not generally true, especially when only satellite  
145 observations are assimilated. In this study, the experiments were further designed to  
146 assimilate surface observations into an imperfect land model.

147 The structure of this paper is arranged as follows: The data and models used in  
148 this study are described in section 2. The details of the WCEnKF-based methods that  
149 incorporate inflation, vertical localization and bias-aware assimilation are provided in  
150 section 3. The experimental designs and evaluations of synthetic experiments are set  
151 in sections 4. The primary results are given in section 5. The discussion and  
152 conclusion comprise sections 6 and 7.

153

## 154 **2. Models and data**

### 155 2.1 Study area

156 The study area is located in the Mongolian Plateau and comprises approximately  
157 9352 square kilometers between 46° and 46.5° N and between 106.125° and 107° E.  
158 The dominant biome is grassland, and no river flows through the area (see Figure 1).

159 The soil moisture content and related meteorological and hydrological parameters  
160 are monitored by automatic stations maintained by the Coordinated Enhanced  
161 Observing Period Asian Monsoon Project (CEOP AP) (Bosilovich and Lawford 2002;  
162 Lawford *et al.* 2004). The CEOP AP was launched by the World Climate Research  
163 Programme (WCRP) to develop an integrated global dataset that can be used to  
164 address issues relating to water and energy budget simulations and predictions,

165 monsoon processes and the prediction of river flows. More details can be found at  
166 <http://www.ceop.net>.

167

## 168 2.2 Forcing data

169 In this study, synthetic experiments were conducted to explore the accuracy of the  
170 assimilation schemes. The simulations were driven by forcing data (including  
171 radiation, wind, pressure, humidity, precipitation and temperature) from the  
172 0.125°x0.125° ERA-Interim dataset (Dee *et al.* 2011) that had been scaled down to  
173 provide a temporal resolution of one hour.

174

## 175 2.3 Models

176 The Common Land Model (CoLM) developed by Dai *et al.* (2003) is a  
177 third-generation land surface model. It combines the best features of three successful  
178 models: the Land Surface Model (LSM, (Bonan 1996)), the Biosphere-Atmosphere  
179 Transfer Scheme (BATS, (Dickinson *et al.* 1993)) and the 1994 version of the Chinese  
180 Academy of Sciences/Institute of Atmospheric Physics model (IAP94, (Dai *et al.*  
181 2003)), and is being further developed. The primary characteristics of the model  
182 include 10 unevenly spaced soil layers (see Table 1), one vegetation layer, 5 snow  
183 layers (depending on the snow depth), explicit treatment of the mass of liquid water,  
184 ice and phase changes within the system of the snow and soil, runoff parameterization  
185 following the TOPMODEL concept, a tiled treatment of the sub-grid fraction of the  
186 energy and water budget balance (Dai *et al.* 2003) and a canopy  
187 photosynthesis-conductance mode that describes the simultaneous transfer of CO<sub>2</sub> and  
188 water vapor into and out of the vegetation. The model parameters include data on the  
189 global terrain, elevation, land use, vegetation, land-water mask and hybrid

190 FAO/STATSGO soil types from the USGS, which are available at a resolution of 30  
191 arc seconds.

192 Version 4.0 of the Community Land Model (CLM 4.0) (Lawrence *et al.* 2011;  
193 Oleson *et al.* 2010) is the land surface parameterization used with the Community  
194 Atmosphere Model (CAM 4.0) and the Community Climate System Model (CCSM  
195 4.0). The CLM 4.0 includes bio-geophysics, the hydrologic cycle, biogeochemistry  
196 and the dynamic vegetation. CLM 4.0 simulates the bio-geophysical processes in each  
197 sub-grid unit independently and maintains its own prognostic variables. The  
198 parameters used in the CLM4.0 differ from those used in the CoLM. For example, the  
199 soil texture data are derived from the IGBP soil data, and the land use data are derived  
200 from the UNH Transient Land Use and Land Cover Change Dataset  
201 (<http://luh.umd.edu/>).

202 In addition to using different parameters, the two models have different structures.  
203 For example, a model of groundwater-soil water interactions (Niu *et al.* 2007; Niu *et*  
204 *al.* 2005) has been incorporated into the CLM 4.0, while zero water flux at the bottom  
205 of a soil column is assumed in the CoLM. Besides, the CLM 4.0 has the same vertical  
206 discretization scheme as the CoLM (see Table 1), which makes comparing the results  
207 of the two models convenient.

208

### 209 **3. Methods**

#### 210 3.1 Forecast and observation systems

211 Using notation similar to that used by Yilmaz *et al.* (2011), the forecast system  
212 can be written as

$$213 \quad \mathbf{y}_{n,t}^f = \mathbf{M}_{n,t-1}(\mathbf{y}_{n,t-1}^a), \quad (1)$$

214 where  $t=1, \dots, T$  is the time index,  $n=1, \dots, N$  represents an ensemble member (in this

215 study, the ensemble size is set to 100),  $\mathbf{M}_{n,t-1}$  is a CoLM forced by the  $n$ -th perturbed  
 216 atmospheric forcing, and  $\mathbf{y}$  is a state vector containing 126 variables. The superscript  
 217 “ $f$ ” and “ $a$ ” specify the forecast and analysis, respectively.

218 Let  $\mathbf{x}$  be the state variables related to the water budget, that comprises of **SM**  
 219 and **SIC** (the soil moisture content and the soil ice content in % at the 10 vertical  
 220 levels listed in Table 1), CWC and SWE (the canopy’s water content and the snow  
 221 water equivalent in kg/m<sup>2</sup>). In this study, only  $\mathbf{x}$  is updated by data assimilation, while  
 222 the model propagates changes to the other variables over time.

223 For the traditional EnKF, the forecast error covariance matrix  $\mathbf{P}_t$  is  
 224 obtained from the ensemble of their anomalies,

$$225 \quad \mathbf{P}_t = \frac{1}{N-1} \sum_{n=1}^N (\mathbf{x}_{n,t}^f - \bar{\mathbf{x}}_t^f) (\mathbf{x}_{n,t}^f - \bar{\mathbf{x}}_t^f)^T. \quad (2)$$

226 where  $\mathbf{x}_{n,t}^f$  is the component of  $\mathbf{y}_{n,t}^f$  related to the water budget,  $\bar{\mathbf{x}}_t^f$  is the ensemble  
 227 mean of  $\mathbf{x}_{n,t}^f$ . To avoid overestimation of the co-variability between shallow  
 228 observations and soil moistures deeper than a threshold layer  $s$  (see section 3.2 for the  
 229 estimation of  $s$ ), the following vertical localization function with weighting of  
 230 observations  $\rho_s$  (Janjić *et al.* 2011) will be applied on  $\mathbf{P}_t$ , i.e.,

$$231 \quad \rho_s(l) = \exp(-\mu_s |d_l - d_o|) \quad (3)$$

232 where  $l$  represents for the  $l$ -level soil layer,  $d_l$  and  $d_o$  represent the depths of  
 233  $l$ -level soil layer and observation, respectively.  $|d_l - d_o|$  is the Euclidian distance  
 234 between the two layers.  $\mu_s$  is estimated by minimizing the following mean square  
 235 error between vertical localization function Eq (3) and a step function with threshold  
 236 layer  $s$ ,



$$M(\mu) = \sum_{l \leq s} [\exp(-\mu |d_l - d_o|) - 1]^2 + \sum_{l > s} [\exp(-\mu |d_l - d_o|)]^2 \quad (4)$$

The estimated  $\mu_s$  is listed in Table 2.

The observations of the soil moisture content are collected at a depth of 3 cm at 6:00 am every day (denoted by  $o_t$ ). The observation system is defined as

$$o_t = \mathbf{h}\mathbf{x}_t + \varepsilon_t, \quad (5)$$

where observational operator  $\mathbf{h}$  is a 22-dimensional vector which linearly interpolated the soil moisture at depths of 2.8 cm and 6.2 cm to depth of 3 cm,  $\mathbf{x}_t$  represents the true values of the state variables related to the water budget at the time step  $t$  and  $\varepsilon_t$  is the observational error with mean zero and variance  $R_t$ . Since, the main objective of this study is for methodology related to linear observational operators. Choosing the linear interpolation as observational operator is only for convenience.

### 3.2 Assimilation with water budget constraint

Assimilating data on the soil moisture content usually results in an imbalance in the water budget. To reduce this imbalance, a weak constraint on the water budget (Yilmaz *et al.* 2011) is adopted in this study. The ensemble water budget residual at time step  $t$  can be expressed as

$$r_{n,t} \equiv \beta_{n,t} - \mathbf{c}^T \mathbf{x}_{n,t}^a, \quad (6)$$

where

$$\beta_{n,t} = \mathbf{c}^T \mathbf{x}_{n,t-1}^a + Pr_t - Ev_{n,t}^f - Rn_{n,t}^f, \quad (7)$$

where  $\mathbf{c}$  is a 22-dimensional vector that converts the units to millimeters ( $mm$ ) and adds up the states in  $\mathbf{x}$ , the diagnostic variables  $Pr_t$ ,  $Ev_{n,t}^f$  and  $Rn_{n,t}^f$  ( $mm$ ) are scalars specifying the states of the precipitation, evapotranspiration and runoff,

260 respectively, in each pixel.

261 The cost function used to estimate the state variables with the weak water budget  
 262 constraint (Eq. (6)) is

$$263 \quad J_{n,t}(\mathbf{x}) = (o_t - \mathbf{h}\mathbf{x})^T R_t^{-1} (o_t - \mathbf{h}\mathbf{x}) + (\mathbf{x} - \mathbf{x}_{n,t}^f)^T \mathbf{P}_{s,t}^{-1} (\mathbf{x} - \mathbf{x}_{n,t}^f) \\ + (\beta_{n,t} - \mathbf{c}^T \mathbf{x})^T \varphi_t^{-1} (\beta_{n,t} - \mathbf{c}^T \mathbf{x}), \quad (8)$$

264 where

$$265 \quad \varphi_t = \frac{1}{N-1} \sum_{n=1}^N \left( \beta_{n,t} - \frac{1}{N} \sum_{j=1}^N \beta_{j,t} \right) \times \left( \beta_{n,t} - \frac{1}{N} \sum_{j=1}^N \beta_{j,t} \right)^T \quad (9)$$

266 is an estimate of the variance of  $\beta_{n,t}$  and  $\mathbf{P}_{s,t}$  represents a forecast error  
 267 covariance matrix defined by

$$268 \quad \mathbf{P}_{s,t} = \left[ \sqrt{\lambda_t} \right] [\boldsymbol{\rho}_s] \mathbf{P}_t [\boldsymbol{\rho}_s] \left[ \sqrt{\lambda_t} \right]. \quad (10)$$

269 where  $\mathbf{P}_t$  is defined as Eq. (2);  $[\boldsymbol{\rho}_s]$  is a diagonal matrix which localizes the soil  
 270 moisture error (i.e. it is  $\boldsymbol{\rho}_s$  defined by Eq. (3) for the soil moisture contents and 1 for  
 271 other variables).  $[\sqrt{\lambda_t}]$  is also a diagonal matrix which inflates the forecast soil  
 272 moisture error (i.e. it is a scalar  $\lambda_t$  for the soil moisture contents and 1 for other  
 273 variable).  $\lambda_t$  is estimated by minimizing the -2log-likelihood of the difference  
 274 between the forecast and the observation (Dee and Da Silva 1999; Liang *et al.* 2012;  
 275 Zheng 2009),

$$276 \quad -2L_{s,t}(\lambda_t) = \ln(\mathbf{h}\mathbf{P}_{s,t}\mathbf{h}^T + R_t) + (o_t - \mathbf{h}\mathbf{x}_t^f)^T (\mathbf{h}\mathbf{P}_{s,t}\mathbf{h}^T + R_t)^{-1} (o_t - \mathbf{h}\mathbf{x}_t^f). \quad (11)$$

277 The estimated forecast error inflation factor is denoted as  $\hat{\lambda}_t$ . The perturbed analysis  
 278 states of the variables related to water budget can be derived by minimizing Eq. (8),  
 279 which has the analytic form

280 
$$\mathbf{x}_{n,t}^a = \mathbf{x}_{n,t}^f + \mathbf{P}_t^a \mathbf{h}^T R_t^{-1} (o_t + \varepsilon_{n,t} - \mathbf{h} \mathbf{x}_{n,t}^f) + \mathbf{P}_t^a \mathbf{c} \varphi_t^{-1} (\beta_{n,t} - \mathbf{c}^T \mathbf{x}_{n,t}^f), \quad (12)$$

281 where  $\varepsilon_{n,t}$  is generated from a normal distribution with mean zero and variance  $R_t$ ,

282 and

283 
$$\mathbf{P}_t^a = \left( \mathbf{h}^T R_t^{-1} \mathbf{h} + \mathbf{P}_{s,t}^{-1} + \mathbf{c} \varphi_t^{-1} \mathbf{c}^T \right)^{-1}, \quad (13)$$

284 its analysis error covariance matrix.

285 For estimating the optimal threshold layer, define the -2log-likelihood of the total  
286 difference between the forecasts and the observations,

287 
$$L_s \equiv \sum_{t=1}^T (-2L_{s,t}(\hat{\lambda}_t)). \quad (14)$$

288 The optimal threshold layer  $\hat{s}$  is selected as the smallest number  $s$  such that  $L_s$  is  
289 the minimum of  $\{L_2, L_3, \dots, L_{s+1}\}$ . The final analysis state is the selected  
290 corresponding to the optimal threshold layer  $\hat{s}$ . The complete assimilation procedure  
291 with water budget constraint is shown in Figure 2.

292

### 293 3.3 Bias-aware assimilation

294 The bias-aware data assimilation proposed by Dee (2005) is adopted to correct  
295 the analysis bias.

296 Let  $\mathbf{b}_t$  is the estimated bias at time step  $t$  and set  $\mathbf{b}_1 = 0$ . For  $t > 1$ ,

297 
$$\mathbf{b}_t = \mathbf{b}_{t-1} - \gamma \tilde{\mathbf{P}}_{s,t} \mathbf{h}^T \left( \mathbf{h} \tilde{\mathbf{P}}_{s,t} \mathbf{h}^T + R_t \right)^{-1} \left( o_t - \mathbf{h}(\tilde{\mathbf{x}}_t^f - \mathbf{b}_{t-1}) \right). \quad (15)$$

298 where the scalar parameter  $\gamma$  that controls the magnitude of the forecast bias is  
299 estimated following Dee and Todling (2000) (see Eqs (A5)-(A6) of Appendix A),  $\tilde{\mathbf{x}}_t^f$

300 is the ensemble mean of the perturbed forecast states  $\tilde{\mathbf{x}}_{n,t}^f$  from the analysis state

301  $\tilde{\mathbf{x}}_{n,t-1}^a$ ,  $\tilde{\mathbf{P}}_{s,t}$  is the corresponding adjusted forecast error covariance (see Eq. (A2) of

302 Appendix A).

303 Then the perturbed assimilated states are

$$\begin{aligned} 304 \quad \tilde{\mathbf{x}}_{n,t}^a = & \tilde{\mathbf{x}}_{n,t}^f - \mathbf{b}_{t-1} + \tilde{\mathbf{P}}_t^a \mathbf{h}^T R_t^{-1} \left( o_t + \varepsilon_{n,t} - \mathbf{h} \left( \tilde{\mathbf{x}}_{n,t}^f - \mathbf{b}_{t-1} \right) \right) \\ & + \tilde{\mathbf{P}}_t^a \mathbf{c} \tilde{\varphi}_t^{-1} \left( \tilde{\beta}_{n,t} - \mathbf{c}^T \left( \tilde{\mathbf{x}}_{n,t}^f - \mathbf{b}_{t-1} \right) \right) \end{aligned} \quad (16)$$

305 where  $\tilde{\beta}_{n,t}$ ,  $\tilde{\varphi}_t^{-1}$  and  $\tilde{\mathbf{P}}_t^a$  are defined by Eqs (A7)-(A9) in Appendix A respectively.

306

## 307 4. Synthetic experiments

### 308 4.1 Experimental design

309 To investigate the performance of the WCEnKF-based methods that incorporate  
310 inflation, vertical local localization and bias-aware assimilation, synthetic experiments  
311 were performed using the CoLM. Unlike the “perfect model” assumption used in  
312 Yilmaz et al. (2011), the assumptions of this study are accounted for the error in the  
313 model, especially the structural error. Because there were structural differences in the  
314 models of the water cycle (see section 2.3) used in the two models, CLM 4.0 was used  
315 to generate the “true values” (i.e., to perform a reference run) for the synthetic  
316 experiments and CoLM was selected as the forecast operator (i.e., to perform an  
317 open-loop run). Therefore, the CLM 4.0 and the CoLM were both integrated on a  
318 0.125° grid (see Figure 1 for the locations) with a time step of one hour. The  
319 assimilation time was set to 6:00 am every day. The assimilation experiments were  
320 conducted with 5 scenarios: the traditional ensemble Kalman filter (EnKF), a weakly  
321 constrained ensemble Kalman filter (WCEnKF), a weakly constrained ensemble  
322 Kalman filter with inflation (WCEnKF-Inf), a weakly constrained ensemble Kalman  
323 filter with inflation and localization (WCEnKF-Inf-Loc) and a weakly constrained  
324 ensemble Kalman filter with inflation, localization and bias-aware assimilation  
325 (WCEnKF-Inf-Loc-BA).

326 Synthetic observations were obtained by interpolating  $\mathbf{SM}_t$  to a depth of 3 cm  
327 and adding noise with a normal distribution ( $N(\mu=0, \sigma=0.5\%)$ ). The initial state  
328  $\mathbf{x}_0$ , was generated by running the CoLM from October 1, 2002 to June 1, 2003. Each  
329 component of the initial state was perturbed using an independent standard Gaussian  
330 random variable times 5% of magnitude of the component. The forcing data were  
331 perturbed in the manner described in Yilmaz et al. (2011). The synthetic experiments  
332 were conducted from June 1, 2003 to October 1, 2003. The state variables for each  
333 pixel were updated independently.

334

## 335 4.2 Validation statistics

### 336 4.2.1 Model error and bias

337 The model errors are defined as the difference between the actual values and the  
338 model's predictions based on true initial values, and the bias is the average of the error  
339 in the model during the relevant period. Let  $x_t$  denote the true values of the soil  
340 moisture content at time  $t$  for a location and vertical soil layer.  $x_t^M$  denotes the model  
341 predicted soil moisture from the true state at the previous time step  $t-1$ . The model's  
342 bias and error variance for one step can be written as

$$343 \quad b_M = \frac{1}{a_{ts}} \sum_{t=1}^{a_{ts}} (x_t^M - x_t), \quad (17)$$

$$344 \quad v_M = \frac{1}{a_{ts}} \sum_{t=1}^{a_{ts}} (x_t^M - x_t)^2, \quad (18)$$

345 where  $a_{ts}$  is the number of time steps over which the observations made at 6:00 am  
346 each day are assimilated.

### 347 4.2.2 Validation of analysis soil moisture

348 The true soil moisture content values from 7:00 am to 5:00 am next day are used  
 349 to validate analysis states. For a location and vertical soil layer, let  $x_{t,h}$  be the true  
 350 soil moisture content at hour  $h$  on day  $t$ , and  $x_{t,h}^f$  represent the forecasted soil  
 351 moisture content at hour  $h$  from analysis state  $x_t^a$  at 6:00 am on day  $t$ . The analysis  
 352 bias is defined as

$$353 \quad b_a = \frac{1}{23a_{ts}} \sum_{t=1}^{a_{ts}} \sum_{h=7}^{29} (x_{t,h}^f - x_{t,h}). \quad (19)$$

354 The analysis error variance is defined as

$$355 \quad v_a = \frac{1}{23a_{ts}} \sum_{t=1}^{a_{ts}} \sum_{h=7}^{29} (x_{t,h}^f - x_{t,h})^2$$

$$= \frac{1}{23a_{ts}} \sum_{t=1}^{a_{ts}} \sum_{h=7}^{29} (x_{t,h}^f - x_{t,h} - b_a)^2 + b_a^2 \quad (20)$$

356 (See Appendix B for the proof)

### 357 4.2.3 Water balance

358 Following Yilmaz (2011), the water budget imbalance at location is evaluated  
 359 using the water balance residual,

$$360 \quad R = \frac{1}{Na_{ts}} \sum_{t=1}^{a_{ts}} \sum_{n=1}^N r_{n,t}. \quad (21)$$

361 where  $N$  is the ensemble size,  $a_{ts}$  is the number of assimilation time steps, and  $r_{n,t}$  is  
 362 the ensemble water budget residual at time step  $t$  as defined in Eq. (6).

363

## 364 5. Results

365 In the synthetic experiments, the magnitudes of the model's bias and error were  
 366 calculated using Eqs (17) and (18), respectively, and are shown in Figure 3. It shows  
 367 that the model's bias was almost negative from Figure 3a. The negative bias in the  
 368 surface layer was the result of a combination of a lower surface roughness and a larger

369 leaf area index in the CoLM; these values led to more soil evaporation and more  
370 canopy interception and could result in a smaller amount of water infiltrating the soil  
371 than the amount modeled using the CLM 4.0. In the CoLM, the porosity of each layer  
372 was less than it was in the CLM 4.0, which retained less water and contributed to the  
373 negative bias of the upper 9 layers. However, the magnitude of the bias increased to 2%  
374 in the bottom layer. The significant difference between the two models at the bottom  
375 layer could be ascribed to their different boundary conditions. Interactions between  
376 the soil moisture content and the ground water at the bottom of the soil column were  
377 modeled in the CLM 4.0 (Oleson *et al.* 2010) but not in the CoLM. The error in each  
378 model (Figure 3b) fluctuated in a manner similar to that of the model’s bias. Unbiased  
379 observations are necessary for correcting bias in a model, which is not possible in  
380 many realistic applications, especially in assimilating remote sensing retrievals. Since  
381 satellite observations of the soil moisture content of deep layers are unavailable, only  
382 removing the bias in shallow layers would introduce error in model dynamics.

383

## 384 5.1 Forecast error inflation and vertical localization

385 In the synthetic experiments, the study domain comprised 40 pixels. At each point  
386 in the grid-scale threshold layer, the localization scale factor  $\mu_s$ , was determined  
387 independently. Therefore, totally 9 sets of experiments with different localization  
388 scale factor (see Table 2) were conducted separately. Among these experiments, the  
389 “optimal” case for each pixel was defined as the case in which the column averaged  
390 analysis error (Eq. (20)) was minimized (shown in Figure 4). According to Figure 4a,  
391 the corresponding threshold layer  $s$  of  $\mu_s$  was generally between 5 and 6 in both  
392 cases, which could be ascribed to the homogeneous soil texture and land cover. In the  
393 WCEnKF-Inf-Loc, there were 19 pixels in which the threshold layers were “optimal,”

394 and the layers selected in the other pixels were suboptimal (most were roughly one  
395 layer away from the “optimal” case). As shown in Figure 4b, the spatial average of the  
396 root analysis error variance (Eq. (20)) of the WCEnKF-Inf-Loc (4.09%) was  
397 comparable with the optimal value (3.84%) even though  $s$  was not selected on the  
398 basis of minimizing the analysis error.

399 The spatial average of the root analysis error variance in each layer in the  
400 schemes with (WCEnKF-Inf-Loc and WCEnKF-Inf) and without (WCEnKF)  
401 inflation are displayed in Figure 5a. Above 36.6 cm, the analysis errors of the schemes  
402 without inflation (6.70%) were substantially larger than those of the schemes with  
403 inflation (2.00%) for the synthetic experiments. This suggested that inflation provided  
404 a better estimate in the layers close to the observation. When no inflation was  
405 performed, the accuracy of the soil moisture content was barely improved over that of  
406 the open-loop (not shown here).

407 By comparing the schemes with (WCEnKF-Inf-Loc) and without (WCEnKF-Inf)  
408 vertical localization, the impact of this approach on the assimilation accuracy in each  
409 layer is shown in Figure 5a. Because the threshold layer of the localization function  
410  $\rho_s$  was layer 6 (36.6 cm) for 28 of the pixels (see Figure 4a), the spatial average of  
411 root analysis error variance of the results of the WCEnKF-Inf-Loc is almost identical  
412 to that of the results of the WCEnKF-Inf for depths above 36.6 cm. In contrast,  
413 inflation increased the analysis error in the soil moisture content of the deep layers in  
414 the WCEnKF-Inf from 6.38% to 12.49%. In this model, the sample error covariances  
415 of the moisture contents of shallow and deep soil were inflated by a factor greater than  
416 6 (the average inflation factor was 6.25). This could lead to larger assimilation errors  
417 for deep soil moisture profiles in the WCEnKF-Inf. Therefore, inflation should be  
418 used with vertical localization to reduce the spurious covariance resulting from the



419 covariance inflation-based approach.

420 As it was in the synthetic experiments, vertical localization (WCEnKF-Inf-Loc)  
421 was helpful in avoiding erroneous estimates of the soil moisture contents at lower  
422 levels (in the WCEnKF-Inf). A comparison of the analysis error at a depth of 3 cm  
423 (i.e., the depth of the assimilated observations was 3 cm) in the models with  
424 (WCEnKF-Inf and WCEnKF-Inf-Loc) and without (WCEnKF) inflation showed that  
425 the inflation technique significantly reduces the analysis error at the depth at which  
426 observations are made.

427 To investigate the role of bias correction, the spatial averaged root analysis error  
428 variance (Eq. (20)) of WCEnKF-Inf-Loc-BA and WCEnKF-Inf-Loc were compared.  
429 According to Figure 5a, the spatial averaged root analysis error variances of the two  
430 schemes were comparable with each other (2.12% for the WCEnKF-Inf-Loc-BA and  
431 2.16% for the WCEnKF-Inf-Loc) in the layers that were shallower than 36.6 cm. This  
432 could be due to that the observations are closer to the shallow layers and the vertical  
433 localization approach is reasonable effective to reduced the bias. However, for the  
434 layers that were deeper than 62.0 cm, the averaged root analysis error of the  
435 WCEnKF-Inf-Loc-BA (6.05%) was less than that of the WCEnKF-Inf-Loc (6.59%).

436

## 437 5.2 The water budget constraint

438 In the synthetic experiment, the weak constraint on the water budget reduced the  
439 water balance residual significantly in each pixel and the results are shown in Figure 6.  
440 It shows that, the spatial average of the water balance residual of WCEnKF scheme  
441 was 0.0487 mm, which was much smaller than that of the EnKF scheme (0.1389 mm).  
442 Therefore, the assimilation scheme with water budget constraint can indeed reduce the  
443 water balance residuals relative to the assimilation scheme without water budget

444 constraint which is consistent with the results of previous studies (Yilmaz *et al.* 2011;  
445 Yilmaz *et al.* 2012). The interquartile range of the water balance residuals in the 40  
446 pixels for the WCEnKF scheme was 0.0042 mm, which was less than half of that for  
447 the EnKF scheme (0.0098 mm). The reduced spread of the water balance residuals  
448 signals a more stable water balance budget with the water budget constraint.

449 The spatial average of the water balance residual for WCEnKF-Inf,  
450 WCEnKF-Inf-Loc and WCEnKF-Inf-Loc-BA was 0.0834 mm, 0.0737 mm and  
451 0.0723 mm, respectively. The corresponding interquartile range was 0.0079 mm,  
452 0.0051 mm and 0.0072 mm, respectively. They are still much smaller than those for  
453 the EnKF scheme, despite there are bit increase than those for WCEnKF. This  
454 demonstrate the weak water budget constraint is still effective in reducing magnitude  
455 and spread of the water imbalance, despite of more complicated assimilation  
456 approaches were associated.

457

## 458 **6. Discussion**

### 459 6.1 Covariance inflation and vertical localization

460 In this study, the cost function used to estimate the state variables with the weak  
461 water budget constraint (Eq. (8)) consists of three parts, which are related with  
462 observations, model forecasts and water residual (Yilmaz *et al.* 2012). It is represented  
463 as a summation of three scalars, no matter how many observations are assimilated.  
464 Therefore, inflating of one scalar (e.g., model forecasts) seems to have the similar  
465 impact as deflating another one (e.g., water residual), particularly the weights  
466 associated in this problem can be shown as function of the ratio of these three scalars.  
467 Specifically, inflation of forecast error covariance has somewhat similar impact with  
468 deflation of the water balance residual covariance. [If the focus of a study or](#)

469 experiment is reducing water balance, WCEnKF could be a better choice and  
470 computationally faster than WCEnKF-Inf and WCEnKF-Inf-Loc schemes.  
471 Accordingly, it is plainly obvious that the water balance residual of the scheme  
472 WCEnKF-Inf is larger than that of the scheme WCEnKF. However, the objective in  
473 this study is to reduce water balance without significantly increasing the analysis error.  
474 Since the analysis errors for WCEnKF in the layers shallower than 36.6 cm are  
475 significantly larger than those for the schemes with inflation, WCEnKF is not  
476 preferred.

477       According to Figure 5a, the covariance inflation improved the estimates of the  
478 soil moisture content in the shallow layers independently of whether vertical  
479 localization was used. This is primarily because the observation operator,  $\mathbf{h}$ , is the  
480 linear operator that was used to interpolate the soil moisture content at depths of 2.8  
481 cm and 6.2 cm to a depth of 3 cm. Then, the likelihood function for the inflation  
482 factor (Eq. (11)) depends only on the observations and predictions of the soil moisture  
483 content in the 2<sup>nd</sup> and 3<sup>rd</sup> layers. The mean value of the inflation factor is 6.25 for  
484 WCEnKF-Inf, indicating that the initial forecast spread is not large enough. This leads  
485 to an improvement in the forecast error statistics in the shallow layers, and to further  
486 improvements in the assimilated soil moisture contents of those layers.

487       However, the soil moisture contents of the deep layers are not directly related to  
488 the inflation factor. Inflating the forecast errors in the deep layers leads to an  
489 overestimation of the corresponding forecast error covariance, and could lead to larger  
490 analysis errors in the deep layers (see WCEnKF-Inf in Figure 5a). Therefore in this  
491 study, the vertical localization approach was developed to prevent soil moisture over  
492 fitting for deep layers. Using all observations for threshold  $s$  is only for model  
493 selection (from the 10 layers), not for fitting parameter. When vertical localization is

494 used, the soil moisture contents of the deep layers are not significantly updated.  
495 Consequently, larger errors are avoided in the deep layers (see WCEnKF-Inf-Loc in  
496 Figure 5a).

497 Comparing to traditional EnKF without inflation and localization, although  
498 mainly the soil moisture contents of layers above the threshold layer (usually the 5<sup>th</sup> or  
499 6<sup>th</sup> layer) were updated at each time step during the assimilation process when the  
500 WCEnKF-Inf-Loc was used, Figure 5a shows that the soil moisture contents of the  
501 layers below the threshold layer, especially the 6<sup>th</sup> and 7<sup>th</sup> layers, are also improved.  
502 This may be because the model propagates changes in the shallow layers downward,  
503 adjusting the soil moisture contents of the deep layers. Because the soil moisture  
504 content of layers above the threshold layer was improved during the previous time  
505 step, this process results in better predictions of the soil moisture contents of layers  
506 below the threshold layer, and therefore, reduces the analysis error in layers below the  
507 threshold layer.

508

## 509 6.2 Bias correction

510 Geophysical models are never perfect and usually produce estimates with biases  
511 that vary in time and in space (Reichle 2008). Therefore, bias correction is important  
512 for assimilating data into models. In this study, only soil moisture in shallow layers  
513 can be observed (in order to mimic the satellite observation), so the bias for the soil  
514 moisture in deeper layers can not be entirely removed only using the observations.  
515 However, bias can be detected by monitoring statistics of observation-minus-forecast  
516 residual in the assimilation systems. Therefore the bias-aware assimilation proposed by  
517 Dee (2005) was further applied to reduce the bias of soil moisture in all layers.

518 For further evaluating the efficacy of the bias-aware assimilation scheme, the

519 analysis error variance was decomposed to a short-lived component (Figure 5b) and a  
520 bias component (Figure 5c) for the synthetic experiment. It shows that for the  
521 bias-blind data assimilation scheme (WCEnKF-Inf-Loc), both short-lived errors and  
522 biases reduce in the layers close to observation, while maintain the similar levels as  
523 those for EnKF for the deeper layers. The covariance inflation can play an important  
524 role in bias reduction. Bias can only be seen during long assimilation period. At an  
525 instant time, bias and error are mixed. For the traditional EnKF, the forecast error  
526 covariance matrix obtained from the ensemble of their anomalies (Eq. (2)) mainly  
527 represents short-lived error, so it has to be inflated to include error related to bias.  
528 Moreover, the bias could be further reduced by the additional bias-aware assimilation.

529 There are other bias estimation approaches in data assimilation. For example,  
530 treating bias as model variables and estimate in assimilation (De Lannoy *et al.* 2007;  
531 Dee and Da Silva 1998), adjusting the state variable of the forecast model not only  
532 their covariance matrix in each forecast step (Zhang *et al.* 2014; Zhang *et al.* 2015),  
533 addressing the biases in the model and observations by rescaling their cumulative  
534 distribution functions (Koster *et al.* 2009; Reichle and Koster 2004). The scheme  
535 proposed here can provide a base line to validate the efficacy of these approaches and  
536 could be further improved after these bias corrections.

537

### 538 6.3 Broader implications

539 In our schemes, the canopy's water content was directly updated by the soil  
540 moisture observations, following the approach of previous studies (Yilmaz *et al.* 2011;  
541 Yilmaz *et al.* 2012). The canopy's water content (CWC) and snow water equivalent  
542 (SWE) are related to the water budget. If the water budget constraint is absent, they  
543 are normally not updated and the vegetation module transports the water into the

544 vegetation layer. However, the present study focused on the assimilation with the  
 545 water budget constraint, then updating CWC and SWE would help to reduce the water  
 546 budget residuals.

547 For the assimilation with the water budget constraint but without update of CWC  
 548 and SWE, the state variables related to the water budget are decomposed as  
 549  $\mathbf{x} = (\mathbf{x}_1, \mathbf{x}_2)$  where  $\mathbf{x}_1$  comprises of SM and SIC,  $\mathbf{x}_2$  comprises of CWC and SWE.  
 550  $\mathbf{c} = (\mathbf{c}_1, \mathbf{c}_2)$  converts the units of  $\mathbf{x} = (\mathbf{x}_1, \mathbf{x}_2)$  to millimeters (mm). The assimilation  
 551 for not update of  $\mathbf{x}_2$  can be achieved by substituting  $\mathbf{x}$  and  $\beta_{n,t}$  in section 3.2 by  
 552  $\mathbf{x}_1$  and  $\beta_{n,t}$  respectively, that is

$$553 \quad \beta_{n,t} = \mathbf{c}_1^T \mathbf{x}_{n,t-1}^a + \mathbf{c}_2^T \mathbf{x}_{n,t-1}^f + Pr_t - Ev_{n,t}^f - Rn_{n,t}^f, \quad (22)$$

554 where  $Pr_t$ ,  $Ev_{n,t}^f$  and  $Rn_{n,t}^f$  are diagnostic variables specifying the states of the  
 555 precipitation, evapotranspiration and runoff, respectively. By this way, the canopy's  
 556 water content are not updated and the vegetation module transports the water into the  
 557 vegetation layer. In this study, the range of the estimated CWCs for all assimilations  
 558 with or without update of  $\mathbf{x}_2$  is only about 0.005 mm. Considering the estimated  
 559 water budget residuals are between 0.05 mm and 0.14 mm and there is no SWE in the  
 560 summer period, we conclude that update of CWC has a little impact on water balance  
 561 in this study.

562 The most computational cost in the assimilation system is on computing the  
 563 localization function at each model grid cell. For the synthetic experiments with  
 564 CoLM model and 40 grids, it takes about 24 hours running on the personal  
 565 workstation. For global data assimilation with  $2^\circ$  resolution it could take about 3  
 566 months. However, the super server and parallel computation can significantly shorten  
 567 the computational time. A regional scale using soil texture or climate regimes can also

568 be used to delineate different regions. By this way, the computational time of global  
569 data assimilation can be further reduced.

570 In the near future, we plan to validate the major conclusions under different soil  
571 conditions and land cover types. Vertical localization, which uses adjacent  
572 observations, should also be tested in future work. More detailed analyses of the bias  
573 correction for assimilating remote sensing retrievals should be performed. The  
574 response of the analytic soil moisture content to weather predictions also needs to be  
575 investigated. Completing these studies should improve the state of research into  
576 land-atmosphere interactions.

577

## 578 **7. Conclusions**

579 In this study, observations of the soil moisture content at a depth of 3 cm were  
580 assimilated using an ensemble Kalman filter with several improvements. Firstly, an  
581 adaptive forecast error inflation based on maximum-likelihood estimation was  
582 adopted to reduce the analysis error. This study supports the idea that the proper form  
583 of the forecast error covariance matrix is crucial for reducing the analysis error near  
584 the layers in which observations are made. Secondly, an adequate vertical localization  
585 for the ensemble-based filter was proposed associated with the forecast error  
586 covariance inflation, to avoid misestimates of the soil moisture contents of deep layers.  
587 Lastly, a constraint on the water balance was used in this study to reduce the water  
588 budget residual substantially without significantly changing the assimilation accuracy.  
589 The experiment results of synthetic study show that the WCEnKF-Inf-Loc  
590 assimilation scheme can reduce the analysis error from 6.70% to 2.00% in the shallow  
591 layers, with both the short-lived analysis error and the analysis bias reduced. It also  
592 leads to a rational water budget residual with spatial average 0.0737 mm, which is

593 much smaller than 0.1389 mm of the EnKF scheme. The bias-aware assimilation  
594 scheme is potentially useful to further reduce the analysis error arising from model  
595 bias.

596

597 **Data availability** The soil moisture observations are available at <http://www.ceop.net>.  
598 The ERA-interim forcing data used in the synthetic experiments is obtained from  
599 <https://apps.ecmwf.int/datasets>.

600

601 **Author Contributions** BD performed the simulations and assimilations. XZ designed  
602 the research. GW analyzed the results. TL collected and preprocessed the data. GW  
603 and XZ prepared the manuscript with contributions from all co-authors.

604

605 **Conflicts of Interest** The authors declare that they have no conflict of interest.

606

607 **Acknowledgement** This study was funded by the the National Key R&D Program of  
608 China (2019YFC1510002, 2015CB953703) and the National Natural Science  
609 Foundation of China (41705086). We would like to thank the Editor and two  
610 anonymous reviewers for their insightful comments in improving the manuscript. We  
611 also thank Drs. Yongjiu Dai and Qingyun Duan for their help in land surface model.

612

## 613 **Appendix A. A bias-aware assimilation scheme**

614 For correcting the bias of the analysis states  $\mathbf{x}_{n,t}^a$  in Eq. (12), the bias-aware  
615 assimilation (Dee 2005) is applied.



616 Let  $\mathbf{b}_t$  is the forecast bias at time step  $t$ , and set  $\mathbf{b}_1 = 0$ . Then

$$617 \quad \mathbf{b}_t = \mathbf{b}_{t-1} - \gamma \tilde{\mathbf{P}}_{s,t} \mathbf{h}^T (\mathbf{h} \tilde{\mathbf{P}}_{s,t} \mathbf{h}^T + R_t)^{-1} (o_t - \mathbf{h}(\tilde{\mathbf{x}}_t^f - \mathbf{b}_{t-1})). \quad (\text{A1})$$

618 where  $\tilde{\mathbf{x}}_t^f$  is the ensemble mean of the perturbed forecast states  $\tilde{\mathbf{x}}_{n,t}^f$  predicted from  
 619 the perturbed analysis state at previous time step  $\tilde{\mathbf{x}}_{n,t-1}^a$ , the forecast error covariance  
 620 matrix is in the form

$$621 \quad \tilde{\mathbf{P}}_{s,t} = \left[ \sqrt{\tilde{\lambda}_t} \right] [\boldsymbol{\rho}_s] \tilde{\mathbf{P}}_t [\boldsymbol{\rho}_s] \left[ \sqrt{\tilde{\lambda}_t} \right], \quad (\text{A2})$$

622 where the localization threshold  $s$  is adopted from the bias-blind scheme documented  
 623 in section 3.2,

$$624 \quad \tilde{\mathbf{P}}_t = \frac{1}{N-1} \sum_{n=1}^N (\tilde{\mathbf{x}}_{n,t}^f - \tilde{\mathbf{x}}_t^f) (\tilde{\mathbf{x}}_{n,t}^f - \tilde{\mathbf{x}}_t^f)^T, \quad (\text{A3})$$

625 and the inflation factor  $\tilde{\lambda}_t$  is estimated by minimizing

$$626 \quad -2\tilde{L}_{s,t}(\tilde{\lambda}_t) = \ln(\mathbf{h} \tilde{\mathbf{P}}_{s,t} \mathbf{h}^T + R_t) + (o_t - \mathbf{h} \tilde{\mathbf{x}}_t^f)^T (\mathbf{h} \tilde{\mathbf{P}}_{s,t} \mathbf{h}^T + R_t)^{-1} (o_t - \mathbf{h} \tilde{\mathbf{x}}_t^f). \quad (\text{A4})$$

627 The scalar parameter  $\gamma$  in Eq. (A1) that controls the magnitude of the forecast  
 628 bias estimates, is derived by

$$629 \quad \gamma = \frac{\mu}{1-\mu} (R_t + \mathbf{h} \mathbf{P}_t \mathbf{h}^T) (\mathbf{h} \mathbf{P}_t \mathbf{h}^T)^{-1}, \quad (\text{A5})$$

630 where  $\mu$  is estimated by minimizing the following objective function (Dee and  
 631 Todling 2000)

$$632 \quad f(\mu) = \sum_n n^2 \left\{ \left[ \left[ 1 - \mu / (1 - (1 - \mu) e^{-2\pi i \Delta t / n}) \right] \left[ \sum_t (o_t - \mathbf{h} \tilde{\mathbf{x}}_t^f) e^{-2\pi i \Delta t / n} \right]^2 (R_t + \mathbf{h} \mathbf{P}_t \mathbf{h}^T)^{-1} \right] - 1 \right\}^2 \quad (\text{A6})$$

633 Then the perturbed analysis states is calculated as

$$\begin{aligned}
634 \quad \tilde{\mathbf{x}}_{n,t}^a &= \tilde{\mathbf{x}}_{n,t}^f - \mathbf{b}_{t-1} + \tilde{\mathbf{P}}_t^a \mathbf{h}^T R_t^{-1} \left( o_t + \varepsilon_{n,t} - \mathbf{h} \left( \tilde{\mathbf{x}}_{n,t}^f - \mathbf{b}_{t-1} \right) \right) \\
&+ \tilde{\mathbf{P}}_t^a \mathbf{c} \tilde{\varphi}_t^{-1} \left( \tilde{\beta}_{n,t} - \mathbf{c}^T \left( \tilde{\mathbf{x}}_{n,t}^f - \mathbf{b}_{t-1} \right) \right)
\end{aligned} \tag{A7}$$

635 where

$$636 \quad \tilde{\beta}_{n,t} = \mathbf{c}^T \tilde{\mathbf{x}}_{n,t-1}^a + Pr_t - Ev_{n,t}^f - Rn_{n,t}^f, \tag{A8}$$

$$637 \quad \tilde{\varphi}_t = \frac{1}{N-1} \sum_{n=1}^N \left( \tilde{\beta}_{n,t} - \frac{1}{N} \sum_{j=1}^N \tilde{\beta}_{j,t} \right) \times \left( \tilde{\beta}_{n,t} - \frac{1}{N} \sum_{j=1}^N \tilde{\beta}_{j,t} \right)^T \tag{A9}$$

638 and

$$639 \quad \tilde{\mathbf{P}}_t^a = \left( \mathbf{h}^T R_t^{-1} \mathbf{h} + \tilde{\mathbf{P}}_{s,t}^{-1} + \mathbf{c} \tilde{\varphi}_t^{-1} \mathbf{c}^T \right)^{-1}, \tag{A10}$$

640

## 641 **Appendix B. Proof of Eq. (20)**

642 For a location and vertical soil layer, the analysis error variance in the synthetic  
643 experiment is defined as

$$\begin{aligned}
v_a &= \frac{1}{23a_{ts}} \sum_{t=1}^{a_{ts}} \sum_{h=7}^{29} \left( x_{t,h}^f - x_{t,h} \right)^2 \\
644 \quad &= \frac{1}{23a_{ts}} \sum_{t=1}^{a_{ts}} \sum_{h=7}^{29} \left( x_{t,h}^f - x_{t,h} - b_a + b_a \right)^2 \tag{B1} \\
&= \frac{1}{23a_{ts}} \sum_{t=1}^{a_{ts}} \sum_{h=7}^{29} \left( x_{t,h}^f - x_{t,h} - b_a \right)^2 + b_a^2 + \frac{2b_a}{23a_{ts}} \sum_{t=1}^{a_{ts}} \sum_{h=7}^{29} \left( x_{t,h}^f - x_{t,h} - b_a \right)
\end{aligned}$$

645 From the definition of analysis bias (Eq. (19)), the last term on the right hand side of  
646 is zero, so Eq. (20) is proved.

647

648 **References**

- 649 Anderson, J.L. and Anderson, S.L., 1999. A Monte Carlo implementation of the  
650 nonlinear filtering problem to produce ensemble assimilations and forecasts.  
651 *Monthly Weather Review*, 127: 2741-2758.
- 652 Bartalis, Z., Wagner, W., Naeimi, V., Hasenauer, S., Scipal, K., Bonekamp, H., Figa, J.  
653 and Anderson, C., 2007. Initial soil moisture retrievals from the METOP-A  
654 Advanced Scatterometer (ASCAT). *Geophysical Research Letters*, 34(20).
- 655 Bauser, H.H., Berg, D., Klein, O. and Roth, K., 2018. Inflation method for ensemble  
656 Kalman filter in soil hydrology. *Hydrology and Earth System Sciences*, 22(9):  
657 4921-4934.
- 658 Bonan, G.B., 1996. Land surface model (LSM version 1.0) for ecological,  
659 hydrological, and atmospheric studies: Technical description and users guide.  
660 Technical note, National Center for Atmospheric Research, Boulder, CO  
661 (United States). Climate and Global Dynamics Div.
- 662 Bosilovich, M.G. and Lawford, R., 2002. Coordinated enhanced observing period  
663 (CEOP) international workshop. *Bulletin of the American Meteorological*  
664 *Society*, 83(10): 1495-1499.
- 665 Chen, F., Crow, W.T. and Ryu, D., 2014. Dual Forcing and State Correction via Soil  
666 Moisture Assimilation for Improved Rainfall-Runoff Modeling. *Journal of*  
667 *Hydrometeorology*, 15(5): 1832-1848.
- 668 Constantinescu, E.M., Sandu, A., Chai, T. and Carmichael, G.R., 2007.  
669 Ensemble-based chemical data assimilation I: general approach. *Quarterly*  
670 *Journal of the Royal Meteorological Society*, 133: 1229-1243.
- 671 Crow, W.T., Chen, F., Reichle, R.H. and Liu, Q., 2017. L band microwave remote  
672 sensing and land data assimilation improve the representation of prestorm soil

673 moisture conditions for hydrologic forecasting. *Geophysical Research Letters*,  
674 44(11): 5495-5503.

675 Crow, W.T. and Loon, E.V., 2006. Impact of incorrect model error assumptions on the  
676 sequential assimilation of remotely sensed surface soil moisture. *Journal of*  
677 *Hydrometeorology*, 7: 421-432.

678 Crow, W.T. and Wood, E.F., 2003. The assimilation of remotely sensed soil brightness  
679 temperature imagery into a land surface model using Ensemble Kalman  
680 filtering: a case study based on ESTAR measurements during SGP97.  
681 *Advances in Water Resources*, 26: 137-149.

682 Dai, Y., Zeng, X., Dickinson, R.E., Baker, I., Bonan, G.B., Bosilovich, M.G., Denning,  
683 A.S., Dirmeyer, P.A., Houser, P.R., Niu, G., Oleson, K.W., Schlosser, C.A. and  
684 Yang, Z.-L., 2003. The Common Land Model. *Bulletin of the American*  
685 *Meteorological Society*, 84(8): 1013-1023.

686 De Lannoy, G.J.M., Reichle, R.H., Houser, P.R., Pauwels, V.R.N. and Verhoest,  
687 N.E.C., 2007. Correcting for forecast bias in soil moisture assimilation with  
688 the ensemble Kalman filter. *Water Resources Research*, 43(9): n/a-n/a.

689 Dee, D.P., 2005. Bias and data assimilation. *Quarterly Journal of the Royal*  
690 *Meteorological Society*, 131: 3323-3343.

691 Dee, D.P. and Da Silva, A.M., 1998. Data assimilation in the presence of forecast bias.  
692 *Quarterly Journal of the Royal Meteorological Society*, 124(545): 269-295.

693 Dee, D.P. and Da Silva, A.M., 1999. Maximum-likelihood estimation of forecast and  
694 observation error covariance parameters. Part I: Methodology. *Monthly*  
695 *Weather Review*, 127(8): 1822-1834.

696 Dee, D.P., Gaspari, G., Redder, C., Rukhovets, L. and Da Silva, A.M., 1999.  
697 Maximum-likelihood estimation of forecast and observation error covariance

698 parameters. Part II: Applications. *Monthly weather review*, 127(8): 1835-1849.

699 Dee, D.P. and Todling, R., 2000. Data assimilation in the presence of forecast bias:  
700 The GEOS moisture analysis. *Monthly Weather Review*, 128(9): 3268-3282.

701 Dee, D.P., Uppala, S.M., Simmons, A.J., Berrisford, P., Poli, P., Kobayashi, S., Andrae,  
702 U., Balmaseda, M.A., Balsamo, G., Bauer, P., Bechtold, P., Beljaars, A.C.M.,  
703 van de Berg, L., Bidlot, J., Bormann, N., Delsol, C., Dragani, R., Fuentes, M.,  
704 Geer, A.J., Haimberger, L., Healy, S.B., Hersbach, H., Hólm, E.V., Isaksen, L.,  
705 Kållberg, P., Köhler, M., Matricardi, M., McNally, A.P., Monge-Sanz, B.M.,  
706 Morcrette, J.J., Park, B.K., Peubey, C., de Rosnay, P., Tavolato, C., Thépaut,  
707 J.N. and Vitart, F., 2011. The ERA-Interim reanalysis: configuration and  
708 performance of the data assimilation system. *Quarterly Journal of the Royal  
709 Meteorological Society*, 137(656): 553-597.

710 Delworth, T.L. and Manabe, S., 1988. The influence of potential evaporation on the  
711 variabilities of simulated soil wetness and climate. *Journal of Climate*, 1(5):  
712 523-547.

713 Dickinson, R.E., Henderson-Sellers, A. and Kennedy, P.J., 1993. Biosphere  
714 Atmosphere Transfer Scheme (BATS) Version 1e as Coupled to the NCAR  
715 Community Climate Model.

716 Dorigo, W.A., Wagner, W., Hohensinn, R., Hahn, S., Paulik, C., Xaver, A., Gruber, A.,  
717 Drusch, M., Mecklenburg, S., van Oevelen, P., Robock, A. and Jackson, T.,  
718 2011. The International Soil Moisture Network: a data hosting facility for  
719 global in situ soil moisture measurements. *Hydrology and Earth System  
720 Sciences*, 15(5): 1675-1698.

721 Dumedah, G. and Walker, J.P., 2014. Evaluation of Model Parameter Convergence  
722 when Using Data Assimilation for Soil Moisture Estimation. *Journal of*

723            *Hydrometeorology*, 15(1): 359-375.

724 El Gharamti, M., Raeder, K., Anderson, J. and Wang, X.G., 2019. Comparing  
725            Adaptive Prior and Posterior Inflation for Ensemble Filters Using an  
726            Atmospheric General Circulation Model. *Monthly Weather Review*, 147(7):  
727            2535-2553.

728 Entekhabi, D., Njoku, E.G., O'Neill, P.E., Kellogg, K.H., Crow, W.T., Edelstein, W.N.,  
729            Entin, J.K., Goodman, S.D., Jackson, T.J. and Johnson, J., 2010. The soil  
730            moisture active passive (SMAP) mission. *Proceedings of the IEEE*, 98(5):  
731            704-716.

732 Evensen, G., 1994. Sequential data assimilation with a nonlinear quasi-geostrophic  
733            model using Monte Carlo methods to forecast error statistics. *Journal of*  
734            *Geophysical Research*, 99: 10143-10162.

735 Gruber, A., Crow, W.T. and Dorigo, W.A., 2018. Assimilation of Spatially Sparse In  
736            Situ Soil Moisture Networks into a Continuous Model Domain. *Water*  
737            *Resources Research*, 54(2): 1353-1367.

738 GUSEV, Y. and Novak, V., 2007. Soil water–main water resources for terrestrial  
739            ecosystems of the biosphere. *J. Hydrol. Hydromech*, 55(1): 3-15.

740 Han, E., Crow, W.T., Holmes, T. and Bolten, J., 2014. Benchmarking a Soil Moisture  
741            Data Assimilation System for Agricultural Drought Monitoring. *Journal of*  
742            *Hydrometeorology*, 15(3): 1117-1134.

743 Janjić, T., Nerger, L., Albertella, A., Schröter, J. and Skachko, S., 2011. On Domain  
744            Localization in Ensemble-Based Kalman Filter Algorithms. *Monthly Weather*  
745            *Review*, 139(7): 2046-2060.

746 Kerr, Y.H., Waldteufel, P., Wigneron, J.-P., Delwart, S., Cabot, F., Boutin, J.,  
747            Escorihuela, M.-J., Font, J., Reul, N. and Gruhier, C., 2010. The SMOS

748 mission: New tool for monitoring key elements of the global water cycle.  
749 *Proceedings of the IEEE*, 98(5): 666-687.

750 Koster, R.D., Guo, Z.C., Yang, R.Q., Dirmeyer, P.A., Mitchell, K. and Puma, M.J.,  
751 2009. On the Nature of Soil Moisture in Land Surface Models. *Journal of*  
752 *Climate*, 22(16): 4322-4335.

753 Kumar, S.V., Peters-Lidard, C.D., Mocko, D., Reichle, R., Liu, Y.Q., Arsenault, K.R.,  
754 Xia, Y.L., Ek, M., Riggs, G., Livneh, B. and Cosh, M., 2014. Assimilation of  
755 Remotely Sensed Soil Moisture and Snow Depth Retrievals for Drought  
756 Estimation. *Journal of Hydrometeorology*, 15(6): 2446-2469.

757 Lawford, R., Stewart, R., Roads, J., Isemer, H., Manton, M., Marengo, J., Yasunari, T.,  
758 Benedict, S., Koike, T. and Williams, S., 2004. Advancing global-and  
759 continental-scale hydrometeorology: Contributions of GEWEX  
760 hydrometeorology panel. *Bulletin of the American Meteorological Society*,  
761 85(12): 1917-1930.

762 Lawrence, D.M., Oleson, K.W., Flanner, M.G., Thornton, P.E., Swenson, S.C.,  
763 Lawrence, P.J., Zeng, X., Yang, Z.-L., Levis, S., Sakaguchi, K., Bonan, G.B.  
764 and Slater, A.G., 2011. Parameterization improvements and functional and  
765 structural advances in Version 4 of the Community Land Model. *Journal of*  
766 *Advances in Modeling Earth Systems*, 3(3).

767 Li, B., Toll, D., Zhan, X. and Cosgrove, B., 2012. Improving estimated soil moisture  
768 fields through assimilation of AMSR-E soil moisture retrievals with an  
769 ensemble Kalman filter and a mass conservation constraint. *Hydrology and*  
770 *Earth System Sciences*, 16(1): 105-119.

771 Liang, X., Zheng, X., Zhang, S., Wu, G., Dai, Y. and Li, Y., 2012. Maximum  
772 likelihood estimation of inflation factors on error covariance matrices for

773 ensemble Kalman filter assimilation. *Quarterly Journal of the Royal*  
774 *Meteorological Society*, 138: 263-273.

775 Loizu, J., Massari, C., Alvarez-Mozos, J., Tarpanelli, A., Brocca, L. and Casali, J.,  
776 2018. On the assimilation set-up of ASCAT soil moisture data for improving  
777 streamflow catchment simulation. *Advances in Water Resources*, 111: 86-104.

778 Lu, H., Koike, T., Yang, K., Hu, Z.Y., Xu, X.D., Rasmy, M., Kuria, D. and Tamagawa,  
779 K., 2012. Improving land surface soil moisture and energy flux simulations  
780 over the Tibetan plateau by the assimilation of the microwave remote sensing  
781 data and the GCM output into a land surface model. *International Journal of*  
782 *Applied Earth Observation and Geoinformation*, 17: 43-54.

783 Lu, H., Yang, K., Koike, T., Zhao, L. and Qin, J., 2015. An Improvement of the  
784 Radiative Transfer Model Component of a Land Data Assimilation System and  
785 Its Validation on Different Land Characteristics. *Remote Sensing*, 7(5):  
786 6358-6379.

787 McColl, K.A., He, Q., Lu, H. and Entekhabi, D., 2019. Short-Term and Long-Term  
788 Surface Soil Moisture Memory Time Scales Are Spatially Anticorrelated at  
789 Global Scales. *Journal of Hydrometeorology*, 20(6): 1165-1182.

790 Miyoshi, T., 2011. The Gaussian approach to adaptive covariance inflation and its  
791 implementation with the local ensemble transform Kalman filter. *Monthly*  
792 *Weather Review*, 139: 1519-1534.

793 Miyoshi, T., Kalnay, E. and Li, H., 2012. Estimating and including observation-error  
794 correlations in data assimilation. *Inverse Problems in Science & Engineering*,  
795 32: 1-12.

796 Niu, G.-Y., Yang, Z.-L., Dickinson, R.E., Gulden, L.E. and Su, H., 2007.  
797 Development of a simple groundwater model for use in climate models and



798 evaluation with Gravity Recovery and Climate Experiment data. *Journal of*  
799 *Geophysical Research*, 112(D7).

800 Niu, G.Y., Yang, Z.L., Dickinson, R.E. and Gulden, L.E., 2005. A simple  
801 TOPMODEL - based runoff parameterization (SIMTOP) for use in global  
802 climate models. *Journal of Geophysical Research: Atmospheres (1984–2012)*,  
803 110(D21).

804 Njoku, E.G., Jackson, T.J., Lakshmi, V., Chan, T.K. and Nghiem, S.V., 2003. Soil  
805 moisture retrieval from AMSR-E. *Geoscience and Remote Sensing, IEEE*  
806 *Transactions on*, 41(2): 215-229.

807 Oleson, K.W., Lawrence, D.M., Gordon, B., Flanner, M.G., Kluzek, E., Peter, J.,  
808 Levis, S., Swenson, S.C., Thornton, E. and Feddema, J., 2010. Technical  
809 description of version 4.0 of the Community Land Model (CLM).

810 Pan, M. and Wood, E.F., 2006. Data assimilation for estimating the terrestrial water  
811 budget using a constrained ensemble Kalman filter. *Journal of*  
812 *Hydrometeorology*, 7(3): 534-547.

813 Pielke, R.A., 2001. Influence of the spatial distribution of vegetation and soils on the  
814 prediction of cumulus Convective rainfall. *Reviews of Geophysics*, 39(2):  
815 151-177.

816 Pinnington, E., Quaife, T. and Black, E., 2018. Impact of remotely sensed soil  
817 moisture and precipitation on soil moisture prediction in a data assimilation  
818 system with the JULES land surface model. *Hydrology and Earth System*  
819 *Sciences*, 22(4): 2575-2588.

820 Raanes, P.N., Bocquet, M. and Carrassi, A., 2019. Adaptive covariance inflation in the  
821 ensemble Kalman filter by Gaussian scale mixtures. *Quarterly Journal of the*  
822 *Royal Meteorological Society*, 145(718): 53-75.

823 Reichle, R.H., 2008. Data assimilation methods in the Earth sciences. *Advances in*  
824 *Water Resources*, 31: 1411-1418.

825 Reichle, R.H. and Koster, R.D., 2004. Bias reduction in short records of satellite soil  
826 moisture. *Geophysical Research Letters*, 31(L19501).

827 Reichle, R.H. and Koster, R.D., 2005. Global assimilation of satellite surface soil  
828 moisture retrievals into the NASA Catchment land surface model. *Geophysical*  
829 *Research Letters*, 32.

830 Robock, A., Vinnikov, K.Y., Srinivasan, G., Entin, J.K., Hollinger, S.E., Speranskaya,  
831 N.A., Liu, S. and Namkhai, A., 2000. The global soil moisture data bank.  
832 *Bulletin of the American Meteorological Society*, 81(6): 1281-1299.

833 Santanello, J.A., Kumar, S.V., Peters-Lidard, C.D. and Lawston, P.M., 2016. Impact of  
834 Soil Moisture Assimilation on Land Surface Model Spinup and Coupled  
835 Land-Atmosphere Prediction. *Journal of Hydrometeorology*, 17(2): 517-540.

836 Wang, X. and Bishop, C.H., 2003. A comparison of breeding and ensemble transform  
837 kalman filter ensemble forecast schemes. *Journal of the Atmospheric Sciences*,  
838 60: 1140-1158.

839 Wei, J., Dirmeyer, P.A., Guo, Z., Zhang, L. and Misra, V., 2010. How Much Do  
840 Different Land Models Matter for Climate Simulation? Part I: Climatology  
841 and Variability. *Journal of Climate*, 23(11): 3120-3134.

842 Wu, G., Zheng, X., Wang, L., Zhang, S., Liang, X. and Li, Y., 2013. A New Structure  
843 for Error Covariance Matrices and Their Adaptive Estimation in EnKF  
844 Assimilation. *Quarterly Journal of the Royal Meteorological Society*, 139:  
845 795-804.

846 Yang, K., Koike, T., Kaihotsu, I. and Qin, J., 2009. Validation of a dual-pass  
847 microwave land data assimilation system for estimating surface soil moisture

848 in semiarid regions. *Journal of Hydrometeorology*, 10: 780-793.

849 Yang, K., Zhu, L., Chen, Y., Zhao, L., Qin, J., Lu, H., Tang, W., Han, M., Ding, B. and  
850 Fang, N., 2016. Land surface model calibration through microwave data  
851 assimilation for improving soil moisture simulations. *Journal of Hydrology*,  
852 533: 266-276.

853 Yang, S.-C., Kalnay, E. and Enomoto, T., 2015. Ensemble singular vectors and their  
854 use as additive inflation in EnKF. *Tellus A*, 67.

855 Yilmaz, M.T., DelSole, T. and Houser, P.R., 2011. Improving Land Data Assimilation  
856 Performance with a Water Budget Constraint. *Journal of Hydrometeorology*,  
857 12(5): 1040-1055.

858 Yilmaz, M.T., DelSole, T. and Houser, P.R., 2012. Reducing Water Imbalance in Land  
859 Data Assimilation: Ensemble Filtering without Perturbed Observations.  
860 *Journal of Hydrometeorology*, 13(1): 413-420.

861 Zhang, S., Yi, X., Zheng, X., Chen, Z., Dan, B. and Zhang, X., 2014. Global carbon  
862 assimilation system using a local ensemble Kalman filter with multiple  
863 ecosystem models. *Journal of Geophysical Research-Biogeosciences*, 119(11):  
864 2171-2187.

865 Zhang, S., Zheng, X., Chen, J., Chen, Z., Dan, B., Yi, X., Wang, L. and Wu, G., 2015.  
866 A global carbon assimilation system using a modified ensemble Kalman filter.  
867 *Geoscientific Model Development*, 8: 805-816.

868 Zhao, L. and Yang, Z.L., 2018. Multi-sensor land data assimilation: Toward a robust  
869 global soil moisture and snow estimation. *Remote Sensing of Environment*,  
870 216: 13-27.

871 Zheng, X., 2009. An adaptive estimation of forecast error covariance parameters for  
872 Kalman filtering data assimilation. *Advances in Atmospheric Sciences*, 26(1):

873 154-160.

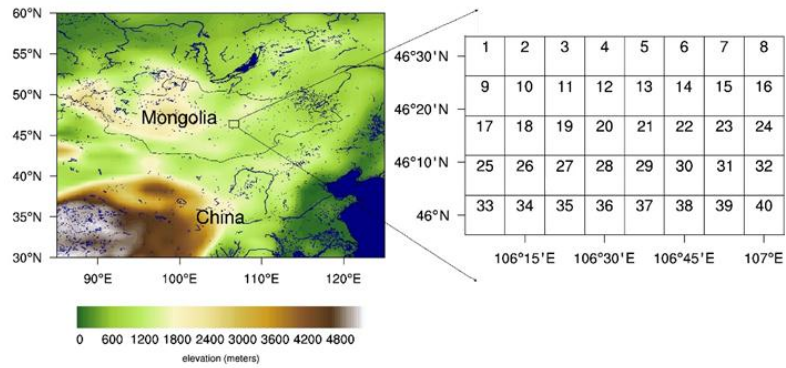
874

875

876 **Figure captions**

877

878



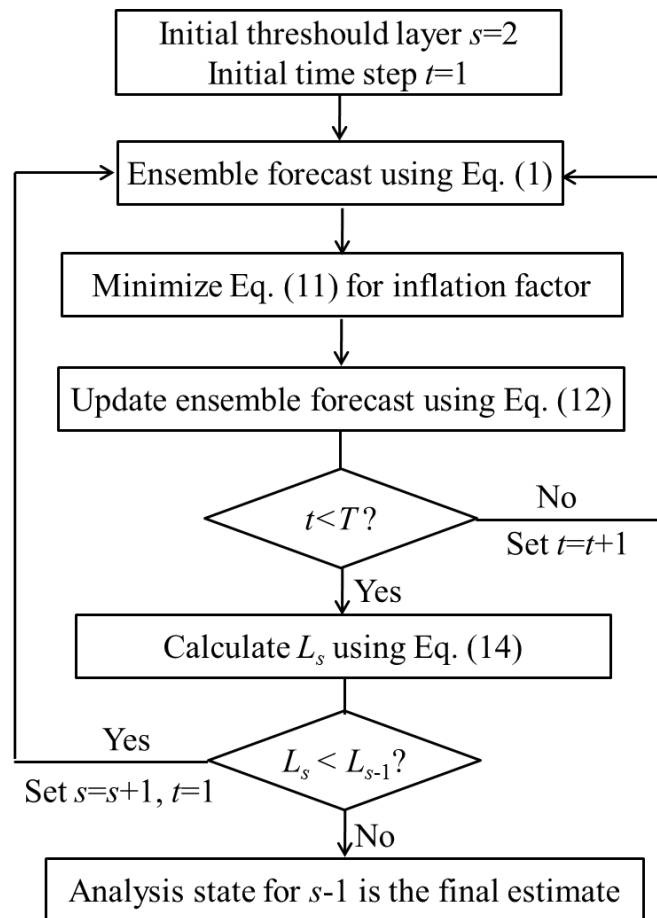
879 Figure 1. The topography and river distribution (left plot) and the geographical

880 location of the synthetic study area (right plot).

881

882

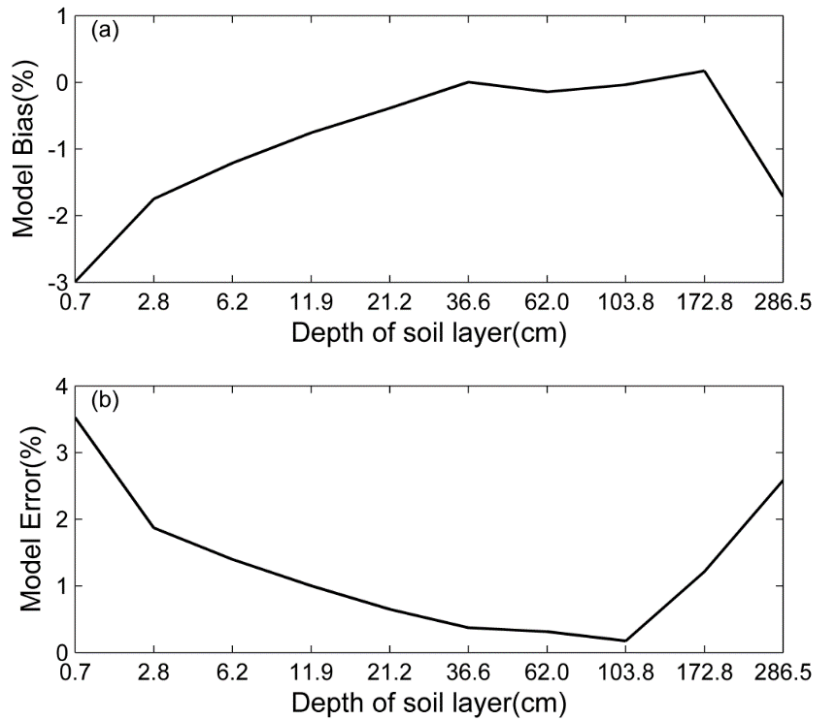
883



884 Figure 2. The assimilation procedure and localization scale factor estimation in the

885 experiments. All of the equations are in accordance with that described in the text.

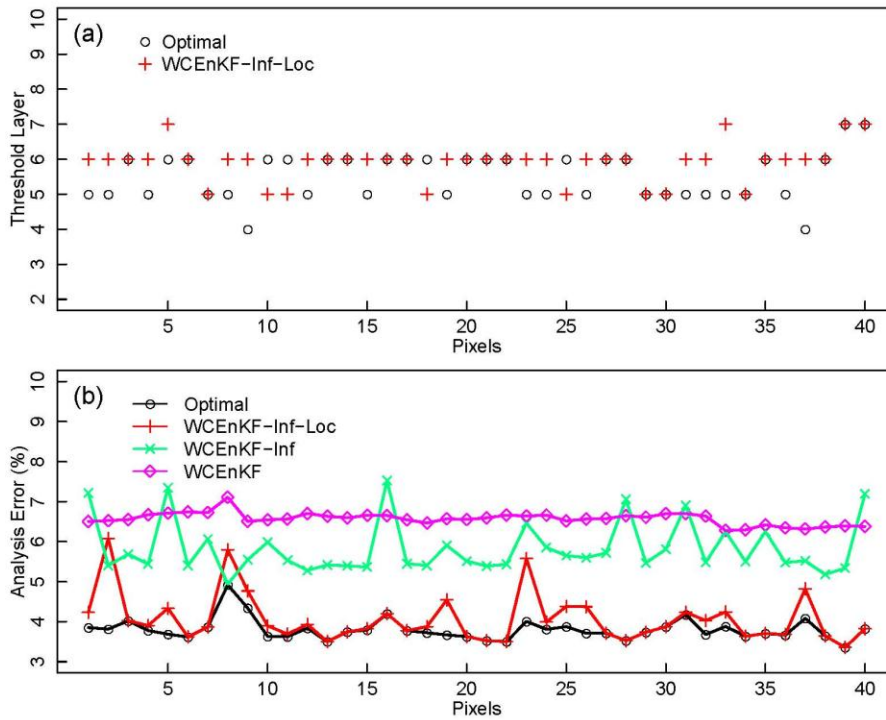
886



887

888 Figure 3. The areal average of the model's bias (a) and error (b) for one step in the soil  
 889 moisture content between the CoLM and the CLM 4.0. The horizontal axis represents  
 890 the layer depth.

891



892

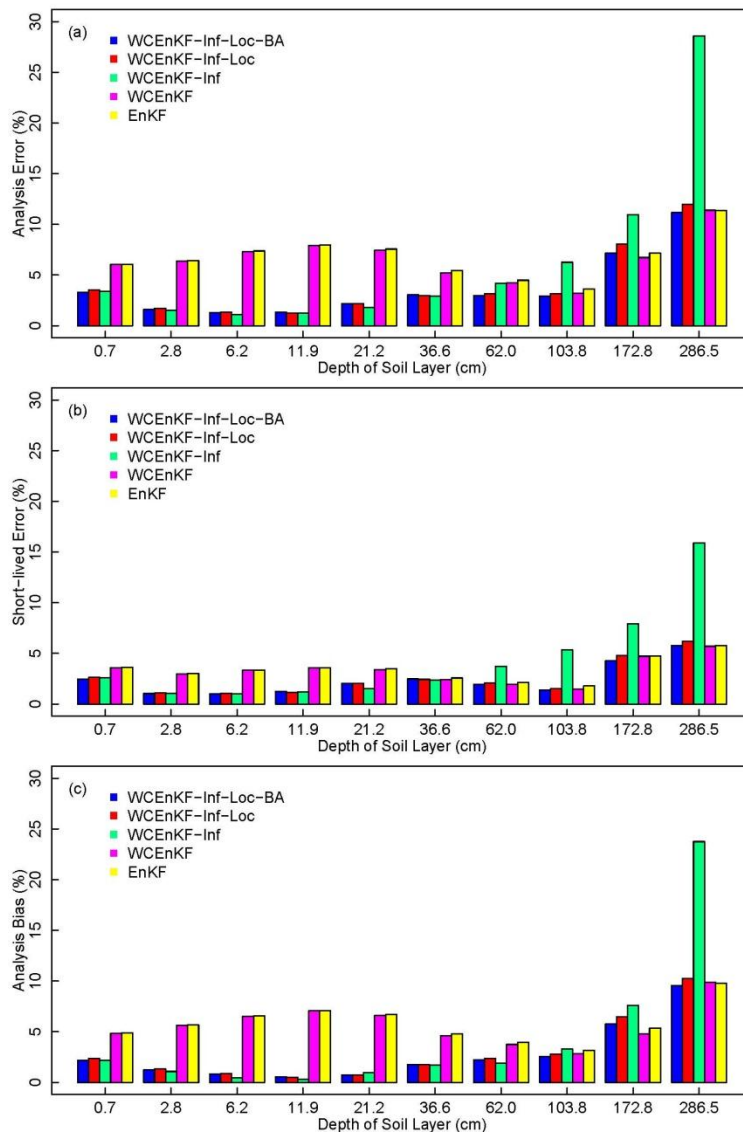
893 Figure 4. The threshold layers and analysis error for each pixel in the synthetic  
 894 experiment. Graph (a) illustrates the optimal and WCEnKF-Inf-Loc threshold layers  
 895 of each pixel. Graph (b) shows the column RSME of each pixel in different schemes  
 896 with water balance constraint (Optimal, WCEnKF-Inf-Loc, WCEnKF-Inf and  
 897 WCEnKF). The horizontal axes of (a) and (b) represent the 40 pixels in the study  
 898 domain.

899

900



901



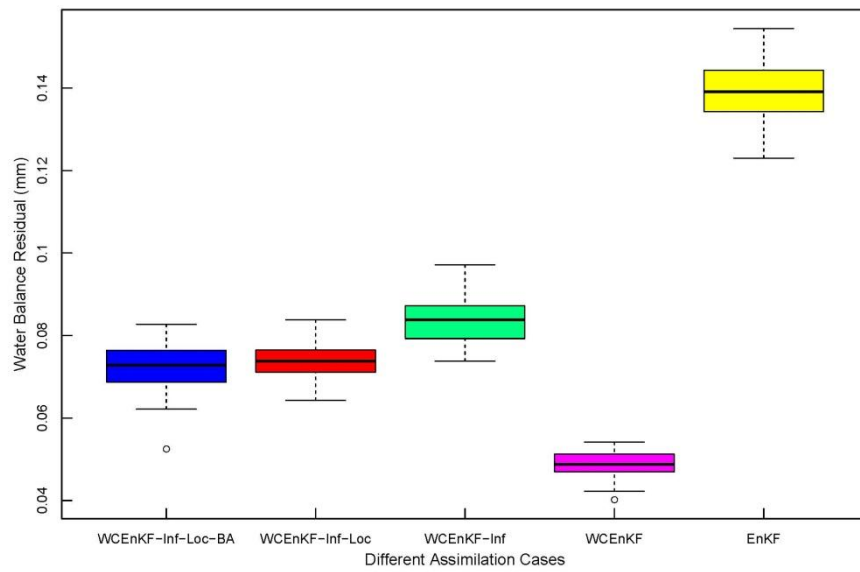
902

903 Figure 5. The assimilation results in each layer for the five schemes: a weakly  
904 constrained bias-aware ensemble Kalman filter with forecast error inflation and  
905 vertical localization (WCEnKF-Inf-Loc-BA), a weakly constrained ensemble Kalman  
906 filter with forecast error inflation and vertical localization (WCEnKF-Inf-Loc), a  
907 weakly constrained ensemble Kalman filter with forecast error inflation  
908 (WCEnKF-Inf), a weakly constrained ensemble Kalman filter (WCEnKF), and the  
909 traditional assimilation (EnKF). Graphic (a) is for spatial averaged analysis error of  
910 the soil moisture content, (b) is for the short-lived error and (c) is for the analysis bias.

911

912

913



914 Figure 6. The box plot of the water balance residual in all 40 pixels for the  
915 WCEnKF-Inf-Loc-BA, WCEnKF-Inf-Loc, WCEnKF-Inf, WCEnKF and EnKF  
916 assimilation schemes.

917

918 Table 1. The node depths (cm) of the 10 soil layers in the CoLM model.

919

Layer	1	2	3	4	5	6	7	8	9	10
Depth (cm)	0.7	2.8	6.2	11.9	21.2	36.6	62.0	103.8	172.8	286.5

920

921

922

923 Table 2. Estimated localization scale factor for different cases.

Layer	2	3	4	5	6	7	8	9	10
$\mu_s$	0.2824	0.1256	0.0587	0.0300	0.0163	0.0093	0.0053	0.0025	0.0001

924